# Pre-deliquescent water uptake in deposited nanoparticles observed with *in situ* ambient pressure X-ray photoelectron spectroscopy

Jack J. Lin,[1] Kamal Raj R,[1] Stella Wang,[2] Esko Kokkonen,[3]
Mikko-Heikki Mikkelä,[3] Samuli Urpelainen,[1,*] and Nønne L. Prisle[1,†]

[1] *Nano and Molecular Systems Research Unit, P. O. Box 3000, FI-90014 University of Oulu, Finland*
[2] *Division of Physics, Math, and Astronomy, California Institute of Technology, Pasadena, California, 91125, USA*
[3] *MAX IV Laboratory, Lund University, Box 118, SE-22100 Lund, Sweden*

(Dated: October 31, 2019)

In this work we study the adsorption, or uptake, of water onto deposited inorganic sodium chloride and organic malonic acid and sucrose nanoparticles at low relative humidities from 0 to 16%. We employ the surface sensitive ambient pressure x-ray photoelectron spectroscopy technique, which has a detection sensitivity from parts per thousand. Our results show that water is adsorbed on sodium chloride aerosols already well below deliquescence at low relative humidities, and that the chemical environment on the aerosol surface is changing with increasing humidity. While the sucrose aerosols exhibit only very modest changes on the surface at these relative humidites, the chemical composition and environment of malonic acid aerosol surfaces is clearly affected. Our observations indicate that the water uptake by inorganic and organic aerosols at low relative humidities could already have an impact on atmospheric chemistry. We also conclude that the ambient pressure x-ray photoelectron spectroscopy is indeed a viable tool for studying changes in particular on the surfaces of atmospherically relevant aerosols at low relative humidities.

Keywords: aerosol, nanoparticles, XPS, ambient pressure XPS, water uptake

## I. INTRODUCTION

The interaction between atmospheric particulate matter, or aerosols, with water is one of the most important processes in Earth's atmosphere. The amount of water associated with an aerosol particle is a function of the hygroscopicity of the particle and the ambient relative humidity (RH). Liquid water composes a significant fraction of the global aerosol mass with field measurements documenting the global presence of the metastable aerosol phase state [1, 2]. Condensed water in the atmosphere influences air quality via light scattering, atmospheric chemistry via the adsorption of gases and promotion of heterogeneous reactions, and climate and hydrological cycle via the activation of dry aerosol particles into cloud droplets [3].

A wide range of techniques are available to study the hygroscopic properties of particles under sub-saturated ($<$ 100% RH) conditions such as humidity-tandem differential mobility analyzers (H-TDMA), various optical extinction and scattering methods, physisorption analyzers, quartz crystal microbalances and even various microscopic and spectroscopic methods [3, 4]. While producing larger quantities of valuable data, the drawback of many of the traditional aerosol techniques such as H-TDMA or optical methods is, when applied alone, that they are not sensitive enough for detecting minute amounts of water adsorbed on the aerosols since both the growth in mass and size are negligible below the deliquescence relative humidity (DRH). Furthermore most of these methods are insensitive to surface-specific chemistry and the phase state of adsorbed water and fail to provide molecular-level information about the system. This can lead to underestimating the amount and importance of water adsorption at low RH.

The equilibrium between the particle phase and water has been experimentally shown to be different for solid and liquid particle [5]. Therefore, knowledge of the particle phase state and humidity history are important parameters for understanding water uptake onto particles. Studying particles at low RH can provide insight into early water uptake and the fundamental nature of hygroscopicity.

A number of spectroscopic techniques have been applied to systems of environmental and atmospheric interest [4, 6]. Using surface-sensitive techniques such as x-ray photoelectron spectroscopy (XPS) provides molecular level information on the chemical composition and properties of surfaces. So far, many of these studies, in particular those employing XPS, have mainly taken the surface science approach and started from the simplified case of single crystal surfaces as an important first step [4]. Experiments on single, isolated aerosol particles are, however, few in number. With the advent of synchrotron radiation and recent developments in electron analyzer technology the barrier of having too low sample density can be overcome and XPS studies can be even performed under realistic conditions, *in situ* and *operando*, using the so called ambient pressure

* Correspondence e-mail address: samuli.urpelainen@oulu.fi
† Correspondence e-mail address: nonne.prisle@oulu.fi

XPS (APXPS) technique [7–9]. In our previous works we have employed the XPS technique to study the solvation of RbBr in free flying water clusters [10] as well as as various aqueous solutions with atmospherically relevant organic surfactants [11–13] as model systems for atmospheric water droplets employing the liquid microjet technique (see e.g. [14].

In this work, we study the pre-deliquescent water uptake of sodium chloride (NaCl), malonic acid, and sucrose. NaCl is a major component of sea salt, the most abundant aerosol by mass in the atmosphere [15]. Organic material composes a large fraction of the ambient aerosol mass [16], and malonic acid and sucrose are two representative, hygroscopic organic compounds. Laboratory-generated particles of each compound were deposited onto substrates for measurement using XPS. Utilizing APXPS, the interaction of the particles with water vapor at the particle surface was studied for relative humidities between 0 and 16%. To the best of our knowledge, this is the first time XPS has been used on nano-scale particles of atmospherically relevant composition.

## II. EXPERIMENTAL

For obtaining information about the chemical composition of the aerosols surfaces APXPS technique was employed. XPS is a surface sensitive technique, where the first few nanometers of a sample are probed by measuring the intensity of photoelectrons emitted from a sample as a function of the electron kinetic energy ($E_k$). When the ionizing photon energy ($h\nu$) is known, the binding energy ($E_b$) can be determined simply as $E_b = h\nu - E_k$. In addition to the binding energy peak areas are also determined. For accurate results for both binding energies and peak areas spectral fitting techniques are employed. Together these parameters give information about the chemical composition and environment (binding energy) and relative abundances of elements (peak area) on the surface of the sample.

The experiments were carried out at the APXPS end station [17, 18] of the SPECIES beamline [19] at the MAX IV Laboratory in Lund, Sweden. In short, the end station is equipped with a hemispherical SPECS Phoibos NAP-150 electron energy analyzer and allows for measurements both at ultra-high vacuum (UHV) conditions as well as up to 25 mbar in an ambient pressure (AP) cell. During the experiments the SPECIES beamline was still under construction and we used a double anode (SPECS XR-50) X-ray source, intended for off-line studies at the end station when synchrotron radiation is not available, with Al (1486.6 eV) and Mg (1253.6 eV) anodes for exciting the samples instead of synchrotron radiation.

The samples deposited on silicon and gold substrates were prepared at the Lund University Aerosol Lab and kept and transferred to the end station in a desiccator in order not to expose them to ambient humidity for extended periods of time prior to the experiments. For the XPS measurements, the substrates were mounted on stainless steel sample holders using an adhesive Cu tape in a clean tent environment and loaded into the end station. The experiments consisted of recording C 1s, O 1s (sucrose and malonic acid), Na 1s and Cl 2p (NaCl) core level XPS spectra of the deposited aerosol particles at UHV and *in situ* at varying RH conditions.

A detailed account of the sample preparation process and conditions as well as the experimental conditions is given in the following sections.

### A. Sample preparation

Aerosol samples were generated by nebulizing solutions of sodium chloride (NaCl), sucrose ($C_{12}H_{22}O_{11}$), and malonic acid ($CH_2(COOH)_2$). The air flow containing solution droplets (3 L $min^{-1}$) was mixed with dry, particle-free air (3 L $min^{-1}$) in a 3 L aerosol mixing chamber. From the mixing chamber, 1–1.5 L $min^{-1}$ was sent through a diffusion dryer followed by a $^{63}$Ni bipolar charger. The dried and charged neutralized particles were either sent to a scanning mobility particle sizer (SMPS; TSI 3936) for size distribution characterization or to a nanometer aerosol sampler (NAS; TSI 3089) for sample collection of the entire dry aerosol size distribution. Sodium chloride particles were collected onto silicon (with native oxide) wafers, while sucrose and malonic acid particles were deposited onto a gold film substrate.

The surface coverage on the substrate is calculated from the geometric mean size $\mu_N$ and total number concentration $N$ measured by the SMPS, the flow rate $Q$ through the NAS, and the total sampling time $t$. The particles are assumed to be spherical across the entire distribution with a charge distribution described by Boltzmann statistics and with 100% deposition efficiency of the positively charged fraction. Coverage is assumed to be uniform with coverage values above 100% indicating the presence of more than one monolayer of deposited particles. Details of the sample generation are given in Table I.

### B. XPS measurements

The UHV XPS spectra were recorded using a pass energy of 50 eV and an entrance slit of 3 mm × 20 mm. This contributes to an experimental broadening of approximately 500 meV in addition to the natural broadening from the excitation source (850 meV for Al $K_\alpha$ and 680 meV for Mg $K_\alpha$ radiation).

Table I. Aerosol sampling data including generated size distribution information and sample collection parameters.

| Compound | Mean Size Distribution | | | | Sample Collection | | | |
|---|---|---|---|---|---|---|---|---|
| | $\mu_N$ (nm) | $\sigma_g$ | N ($cm^{-1}$) | $\mu_{SA}$ ($nm^2$) | Q (L $min^{-1}$) | t (min) | Substrate | Coverage (%) |
| Sodium chloride | 72 | 2.0 | $3.94 \times 10^5$ | 195 | 1.1 | 42 | Si | 232 |
| Sucrose | 79 | 2.2 | $3.59 \times 10^4$ | 202 | 1.1 | 90 | Au | 56 |
| Malonic acid | 52 | 2.1 | $1.02 \times 10^5$ | 193 | 1.2 | 275 | Au | 245 |

For measurements at humid conditions, samples were transferred from the UHV manipulator to the AP cell. Milli-Q water vapor was let into the AP cell through a high precision leak valve, and the pressure inside the cell was kept constant using a valve connected to a pump in a feedback loop with a absolute capacitance manometer. All measurements were made at 25 °C at which the saturation vapor pressure of water $P_{\text{sat}} = 31.73$ mbar. Relative humidity in the cell was calculated using the vapor pressure inside the AP cell pressure so RH = $P_{\text{cell}}/P_{\text{sat}}$. While samples were inside the cell, spectra were recorded at different water vapor pressure conditions (NaCl: 0, 2, 5, and again at 0 mbar; sucrose 0.2, 1, and 5 mbar; malonic acid 0.2 and 1 mbar) at room temperature. The water vapor pressures of 0, 0.2, 1, 2, and 5 mbar correspond to relative humidities of 0, 0.63, 3.2, 6.3, and 16%, respectively. These relative humidities are well below the DRH for NaCl (75.3% [20]), malonic acid (72.1% [21]), and sucrose (85.7% [22]). Any remaining air was removed from the water by several freeze-pump-thaw cycles before introducing the vapor into the AP cell. The cell was also purged with dry nitrogen gas in order to remove any excess water after the experiment. In the case of NaCl, the sample was heated up to 125 °C using a button heater placed behind the sample holder. This was done after the sample was dosed up to 10 mbar to see if the changes after exposure to water vapor were reversible. Spectra obtained at 10 mbar are not included in analysis, however, due to very low signal to noise ratios.

The electron count rates inside the AP cell are reduced when compared to measurements in UHV due to the attenuation of x-ray intensity by the $SiN_3$/Al window, the limited aperture of the differential pumping of the electron analyzer and scattering of the photoelectrons from the vapor[18]. In order to increase the count rate, spectra recorded inside the cell were acquired at a pass energy of 100 eV instead of 50 eV as in the case of UHV in order to compensate for the reduced intensity. The analyzer broadening when using 100 eV pass energy was approximately 1.00 eV. Each spectrum was recorded 50-100 times in static conditions for increased statistics and averaged in time for the final representation.

### C. Data Analysis

Spectral fitting techniques were employed in order to accurately determine the binding energies of the core electrons and the relative amounts (by determining corresponding XPS peak areas) of elements under different conditions. Data analysis was performed using Igor Pro (WaveMetrics, Inc, Lake Oswego, OR, USA). A Shirley-type background was removed from the data before fitting the peaks using the SPANCF curve fitting macro package [23, 24]. All spectra were fitted using symmetric Voigt line shapes. A linear background was included in all the fits to remove any residual background after the Shirley-type background removal. The energy scales of the spectra were calibrated using the well known values of Si 2p (NaCl) and Au 4f (malonic acid and sucrose) for the silicon and gold substrates as the low aerosol particle coverage allowed simultaneous measurement of the substrate.

Before extracting relative ratios for the areas of the core level peaks, the spectra were normalized to the photoionization cross section [25] of the given core electron and attenuation due to scattering of the photoelectrons from the water vapor. The attenuation needed to be taken into account as the fixed excitation energy from the x-ray source leads to significantly different kinetic energies of the emitted photoelectrons, which have different mean free paths in the vapor environment. The attenuation of electron intensity was estimated by using the kinetic theory formulation [8] and measured electron scattering cross section data [26].

## III. RESULTS AND DISCUSSION

The experimental XPS spectra as well as details and results of curve fitting for deposited NaCl, sucrose and malonic acid aerosol particles are presented below. Binding energy shifts from the dry conditions, indicating changes in the chemical environment of the target element, of varying degree are observed with increasing relative humidity. In addition changes in the stoichiometry, or intensity ratios between different core level XPS peaks, of the compounds can be seen. This is a sign of changes in the chemical composition of the molecules themselves on the surface of the aerosol. These observa-

tions are clear indications of water being adsorbed onto and interacting with the particles already at these low relative humidity conditions. The implications and possible interpretations of the observations are discussed below.

### A. NaCl

Figure 1 and Figure 2 show the recorded Na 1s and Cl 2p spectra of NaCl aerosols deposited on a Si substrate measured at 0, 2, 5, and again at 0 mbar (0, 6.3, 16, and 0% RH, respectively) water vapor pressures. The spectra recorded at UHV have been omitted from the figures. The Na 1s spectra were fit using a single, symmetric Voigt peak, except for the 0 mbar spectrum after water exposure, where two peaks were required in order to obtain a fit that represents the measured spectrum. The Cl 2p spectra were fitted with two spin-orbit components.

After calibrating the energy scale using the Si 2p peaks as described earlier, the binding energy of Na 1s core level at UHV conditions was determined to be 1073.48 eV (indicated by the dashed vertical line in Figure 1). The signal-to-noise ratio in the spectra recorded at 5 mbar (16% RH) is very low and the fit line should be regarded more as guiding the eye than an accurate fit of the peak. The binding energy of Cl 2p 3/2 component at UHV conditions was determined to be 200.3 eV (shown by the dashed vertical line in Figure 2).

Figure 3 shows the binding energy shifts of the Na 1s and Cl 2p core level peaks as a function of water vapor pressure at room temperature. There is already a significant shift of approximately 1.1 eV in both the Na 1s and Cl 2p binding energies when water vapor is introduced into the system at very low relative humidities. After this rapid decrease of binding energy, the Cl 2p binding energies show a plateau, when the relative humidity is increased to 16%. The binding energy shift for Na 1s and Cl 2p going from 0% to 6.3% RH is nearly identical, but the shift for Na 1s going from 6.3% to 16% RH is towards larger binding energies by 0.17 eV, while the Cl 2p shifts towards lower binding energies by -0.26 eV. The binding energy shifts are in good agreement with those reported for Na 2s and Cl 2p in NaCl (001) single crystal surfaces by Verdaguer *et al.* [27] showing even a plateau similar to that observed by in the present work. As they did not report the magnitude of the binding energy shift in going from 0 to 5% RH, we have shifted the 5% RH data point of Verdaguer *et al.* to coincide with our data and show their data in Figure 3 as well for easier qualitative comparison of the two. The shift of the Na 1s peak towards larger binding energies at 16% RH in the present data is not entirely in line with the observations on NaCl (001) that show monotonic binding energy shifts towards lower binding

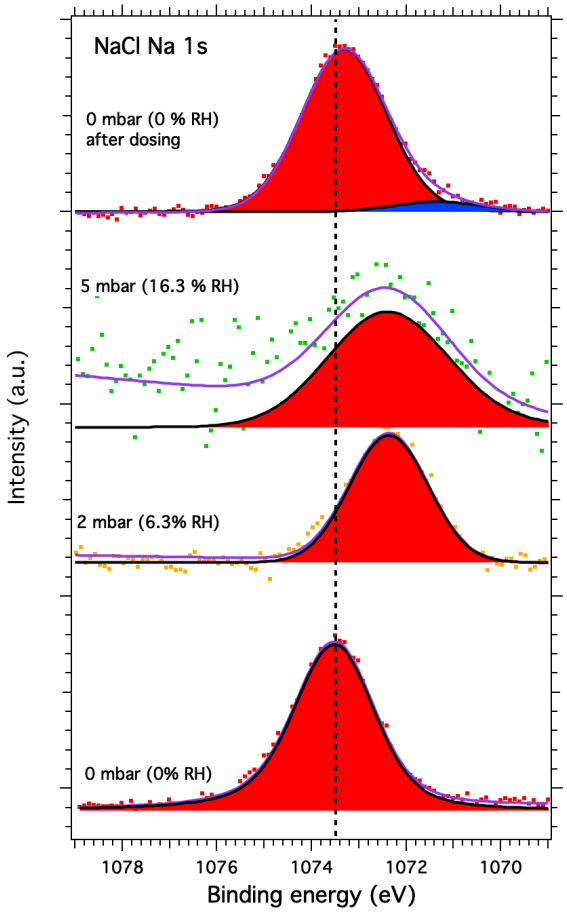


Figure 1. Na 1s XPS spectra of NaCl aerosol particles recorded at different water vapor pressures (relative humidities). The dots show the recorded data, the solid lines the fit envelope curve and the red and blue peaks the fitted Voigt profiles. The dashed vertical line shows the binding energy of Na 1s at 0 mbar pressure (0% RH) in the beginning of the experiments.

energies both for Na 2s and Cl 2p peaks. However, it should be noted that the poorer quality of the experimental spectrum of Na 1s in the present work at 16% RH compared to spectra recorded at lower RH leads to larger uncertainty in the peak fitting procedure. In addition, the shifts obtained in the present work are larger for the Cl 2p than the Na 1s as opposed to larger shifts (by approximately 50 meV) for the Na 2s than the Cl 2p in the NaCl (001) case. After the measurements at 16% RH, the water vapor was removed from the AP cell and another spectrum was recorded at 0% RH. When going from 16% RH to 0% RH, the binding energies of the Na 1s and Cl 2p do not shift back to their original values, but a memory effect of approximately 0.2 eV for Na 1s and Cl 2p is observed. This is in line with the observations by Verdaguer *et al.* who also report a memory effect of less than 0.5 eV.

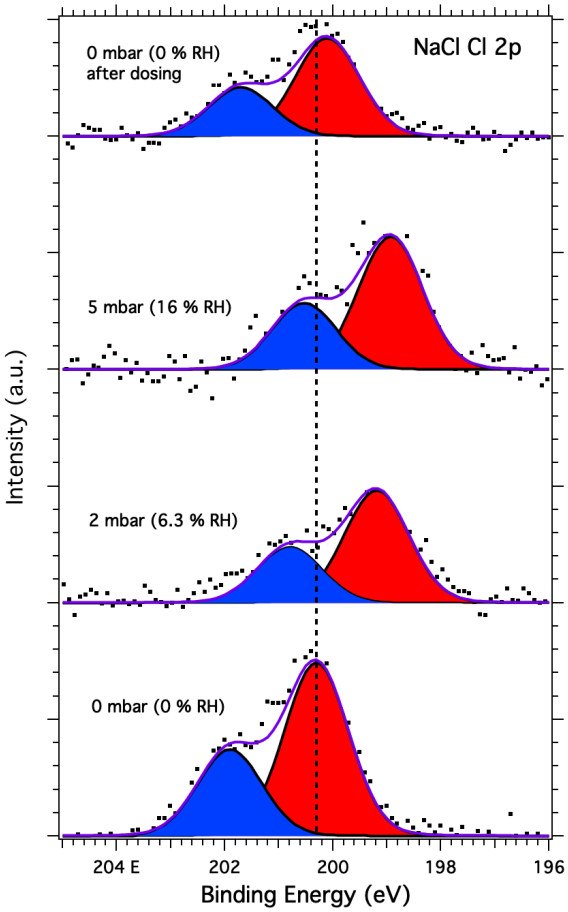


Figure 2. Cl 2p XPS spectra of NaCl aerosol particles recorded at different water vapor pressures (relative humidites). The dots show the recorded data, the solid lines the fit envelope curve and the red and blue peaks the fit 3/2 and 1/2 spin-orbit components, respectively. The dashed vertical line shows the binding energy of Cl 2p 3/2 component at 0 mbar pressure (0% RH) in the beginning of the experiments.

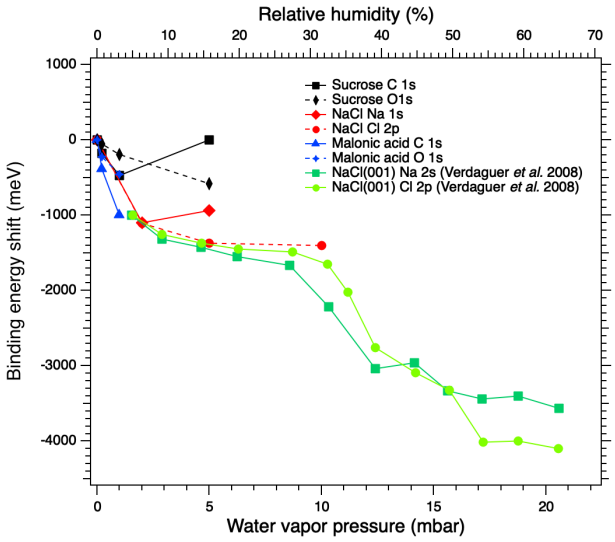


Figure 3. Binding energy shifts of the core level peaks for NaCl, sucrose and malonic acid as a function of water vapor pressure (relative humidity). The green/light green plots extending above 60% RH show the data from Verdaguer *et al.* that has been aligned to the shifts obtained in this study.

In addition to the shifts in binding energies, we also investigated the effects of water vapor on the width of the XPS peaks that could be an indication of changes in the chemical environment or charge carrier mobility on the surface of the aerosols. While we observed clear binding energy shifts, we did not see any significant changes in the peak width of the Na 1s or the Cl 2p peaks. However, the data obtained by Verdaguer *et al.* shows that the total widths of Na 2s and Cl 2p peaks of NaCl (001) single crystal decrease with increasing relative humidity, following qualitatively the behavior of the observed core level binding energy shifts. The difference could be, at least partially, explained by the experimental resolution, which in the present study is lower with peak widths being dominated by experimental factors. In the NaCl (001) case the observed binding energy shifts are attributed to the discharging of the surface: Increasing relative humidity leads to the surface being gradually discharged due to ionized water vapor and secondary electrons. As water is adsorbed onto the surface it will lead to the solvation of surface ions and increased mobility of these charge carriers. This ion mobility makes discharging more efficient leading to further shifts in observed binding energies. According to Verdaguer *et al.* these solvation effects become more significant after approximately 35% RH. This interpretation is further supported by scanning force microscopy studies and infrared studies that show modifications in the surface structure and sudden increase of water coverage at around 40% RH [28–30]. Kelvin probe microscopy (KPM) experiments by Cabrera-Sanfelix *et al.* and Verdaguer *et al.* [27, 31, 32] show how the water vapor affects the surface potential of NaCl(001) surface. They found variations in the order of 0.1 V to 0.25 V in the RH range of their experiments, which clearly is not enough to explain the energy shifts alone. Instead these variations will affect the broadening of the peaks as photoelectrons from different areas of the surface feel a different potential and therefore are slightly shifted. The decrease in peak broadening is attributed to adsorbed water reducing the inhomogeneities in the surface potential. These inhomogeneities originate from potential differences between and within the step and terrace sites of the crystal. The KPM experiments show that the inhomogeneities are removed immediately after water is adsorbed on the surface. In the present work however the deposited aerosol particles are not perfect crystals

and they contain a large number of steps, terraces and kinks, possibly leading to larger variations in the surface potential and thus increased broadening of the peaks. This could, together with the modest experimental resolution, explain why no decrease in the broadening of the peaks is observed for real aerosol particles at low RH.

Apart from the binding energy shifts a decrease in the relative amounts of Na and Cl, or Na 1s to Cl 2p peak area ratio, is also observed even after taking differences in photoionization cross section and attenuation due to scattering in the water vapor into account. This change as a function of increasing RH is presented in Figure 4. The extracted Na to Cl ratio of 0.9 at 0% RH is very close to the expected stoichiometric ratio of 1. However, when the RH is increased to 6.3% and 16%, the ratio clearly decreases to 0.6 and 0.8, respectively. This is another indication of water being adsorbed to the surface as there is a correlation between changes in the chemical composition of the surface layer and RH. Assuming that the distance of the adsorbed water molecules from the NaCl surface is approximately 2.4 Å [31], the photoelectrons emitted from the surface of NaCl need to go through a 2.4 Å layer and would be attenuated by collisions with the water molecules in the process. In our experimental conditions the photoelectrons have kinetic energies (rounded to the nearest ten) of approximately 410 eV and 1290 eV for Na 1s and Cl 2p, respectively. This means that the two core level signals will be attenuated differently due to the different inelastic mean free paths of the electrons (approximately 2 nm and 5 nm, respectively [33]). To quantify the attenuation, an exponential decay $I_n = I_n^0 e^{-x/\lambda_n}$ is used, where $I_n$ is the attenuated intensity of peak $n$, $I_n^0$ is the unattenuated intensity, $x$ is depth of origin of the signal and $\lambda_n$ the inelastic mean free path of peak $n$. Taking the ratio of two peaks 1 and 2 and solving for $x$, the depth of origin becomes $x = \frac{\lambda_1\lambda_2}{\lambda_1-\lambda_2}\ln R$, where $R = \frac{I_1 I_2^0}{I_2 I_1^0}$ is the relative ratio of the two signals. In the present case ($I_1^0/I_2^0 = 0.9$, measured without water vapor), this simple attenuation model gives depths of origin (or water layer thickness) of approximately 1.4 and 0.4 nm for 6.3 and 16% RH, respectively. This is clearly not in line with the previous observations of 2.4 Å and also counterintuitive as the layer thickness would decrease with increasing RH. Furthermore this attenuation model assumes at least a full monolayer coverage so that all signal is attenuated by the adsorbed water layer. Previous studies on NaCl (100) [29, 30, 34] have shown that full monolayer does not develop until RH of approximately 35%. On the other hand, it has been shown that NaCl (100) does not adsorb water strongly whereas small particles (1-10$\mu$m) have a propensity for adsorbing large amounts of water [35]. This strong adsorption has also been connected to the water remaining on the surface even at elevated temperatures in vacuum. Indeed, this is also observed in the present work in the form of a memory effect, of the Na 1s and Cl 2p peak shifts, when going back to RH 0%: the shift does not completely disappear even after heating the sample to 125 °C. Therefore the signs of stronger water adsorption in the present work could be attributed to the small size of our particles contributing to larger surface area and therefore to a larger number of possible adsorption sites.

While attenuation observed due to the adsorbed water layer is one possible explanation for the decreasing Na to Cl ratio observed in this work, another, complementary, explanation could be the dissolution of $Cl^-$ ions into the water film. This should further enhance the difference in the attenuation between Na 1s and Cl 2p XPS signals. In this case the Cl 2p photoelectrons no longer need to pass through the entire water layer while the Na 1s electrons will be attenuated by a layer of water and the dissolved $Cl^-$ ions themselves as well. This interpretation is supported by the density functional theory (DFT) calculations and contact potential measurements [31], which showed that $Cl^-$ can indeed be lifted out of the NaCl (100) surface already at one monolayer water coverage. The presence of halide ions, especially $Cl^-$ and $Br^-$, in the air-water interface has been connected to increased photochemical activity (see e.g Ref. [36] and references therein). This together with the observations presented here indicates that nanoscale NaCl aerosols have the potential of influencing the atmospheric chemistry already at very low RH conditions.

### B. Sucrose

Figure 5 shows the C 1s XPS spectra of deposited sucrose aerosol particles. The C 1s spectra were fitted with three peaks corresponding to C-C/C-H, C-O and O-C-O bonds at 285.24 eV, 286.90 eV, 288.30 eV, respectively, at 0% RH. Sucrose contains only C-O and O-C-O bound carbon and the largest peak corresponding to C-C/C-H bound carbon arises from the adventitious carbon, a thin layer of materials containing carbon that forms on samples exposed to ambient air, on the substrate. During fitting of the spectra, the separation between the C-O and O-C-O peaks was fixed to 1.4 eV, based on previous XPS studies of disaccharides by Stevens *et al.* [37], at all UHV vacuum conditions below $10^{-18}$ mbar. The C-O and O-C-O peaks were however not linked to the peak arising from C-C as there are no purely C-C bound carbon in sucrose. The intensity ratios of the peaks were left unconstrained, but all peaks were forced to have the same symmetric Voigt line shape as the line shape is expected to be dominated by the natural broadening of the Mg $K_\alpha$ x-ray emission lines (680 meV) and the instrumental broadening of the

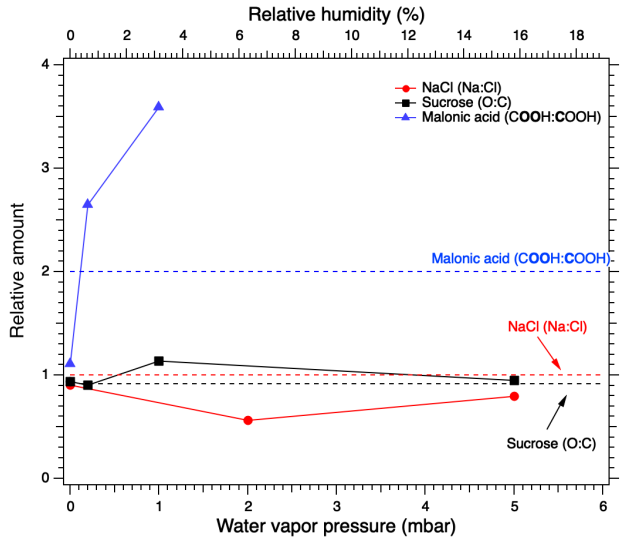


Figure 4. Relative peak areas for NaCl (Na:Cl, red circles), sucrose (O:C, black squares) and malonic acid (C**OO**H:**C**OOH, blue triangles). The dashed horizontal red, black and blue lines show the expected stoichiometric ratio for NaCl, sucrose and malonic acid, respectively. Relative ratios differing from the stoichiometric ratio indicate changes in the chemical composition of the surface of the aerosol.

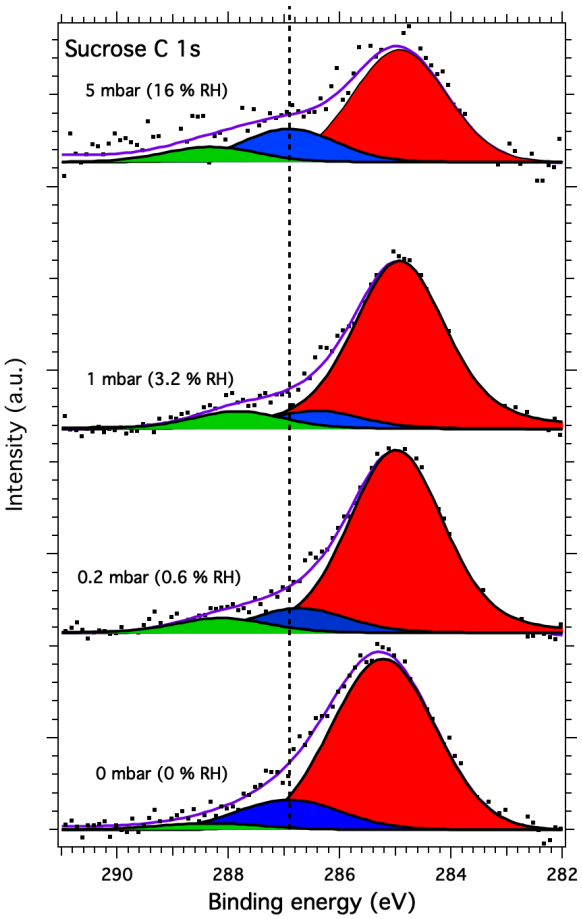


Figure 5. C 1s XPS spectra of sucrose aerosol particles. The dots show the recorded data, the solid lines the fit envelope curve and the red, blue and green peaks the C-C/C-H, C-O and O-C-O components, respectively. The dashed vertical line shows the binding energy of the C-O component at 0 mbar pressure (0% RH) in the beginning of the experiments.

electron analyzer (approximately 1000 meV). The obtained peak energies at 0% RH for C-O and O-C-O are in good agreement with values reported by Stevens *et al.* (286.7 eV and 288.1 eV, respectively).

Figure 6 shows the O 1s XPS spectra of the deposited sucrose aerosol particles. The O 1s spectra were fitted with two (C-O and O-C-O) peaks for sucrose and one peak for the water vapor. The separation between C-O and O-C-O peaks was fixed at 0.7 eV in all relative humidity conditions[37]. Both peaks were fixed to have the same symmetric line shape. The third peak in the XPS spectra measured in humid conditions is the O 1s signal from the water vapor. The binding energies of the C-O and O-C-O peaks at 0% RH were determined to be 532.39 eV and 533.09, respectively. These values differ slightly from those reported by Stevens *et al.* (533.0 eV and 533.7 eV, respectively).

The binding energy shifts of C 1s and O 1s peaks with respect to 0% RH are shown in Figure 3. The C 1s shows initially a small shift and then returns to 0 at 16% RH. The O 1s peaks on the other hand seem to shift slightly towards (580 meV at 16% RH) lower binding energies. Since the separation between the C-O and O-C-O peaks was fixed, they both exhibit the same shift as RH is increased. Figure 4 shows the O to C ratio of sucrose as a function of RH. The ratio oscillates around, and very close to, the stoichiometric value of O:C= $11/12 \approx 0.92$. Looking at the relative ratios of C-O and O-C-O bound carbon C 1s and oxygen O 1s peaks, we see only minor changes. The C-O C 1s signal seems to increase slightly when going from 0% to 3.2% RH, but is again lower at 16% RH. The same is true for O 1s O-C-O signal, which increases slightly towards 16% RH. Considering that both the O 1s and C 1s peaks only show a small binding energy shift with increasing RH, the O:C ratio remains nearly constant and the changes in relative ratios between C-O and O-C-O bound carbon C 1s and oxygen O 1s signals are small, it seems that either there is no significant amounts of water adsorbed at RH below 16% or that if water is adsorbed, there is very little chemical interaction with the water and the aerosol particle.

The observations are well in line with the results of Zobrist *et al.* [38] and others [22]. Zobrist *et al.* used optical techniques in determining the size of single su-

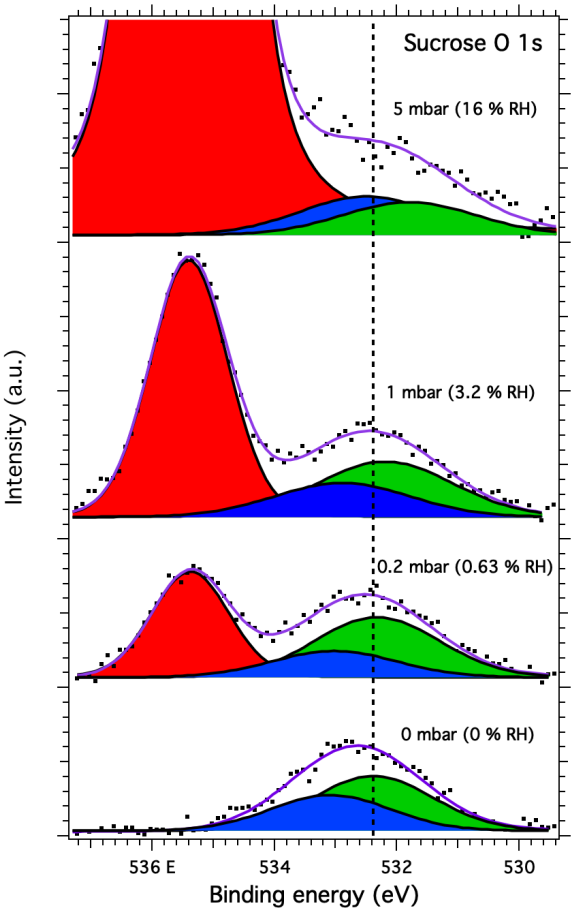


Figure 6. O 1s XPS spectra of sucrose aerosol particles. The dots show the recorded data, the solid lines the fit envelope curve and the red, blue and green peaks the water vapor, and sucrose O-C-O and C-O components, respectively. The dashed vertical line shows the binding energy of the C-O component at 0 mbar pressure (0% relative humidity) in the beginning of the experiments.

crose microparticles levitated in an electrodynamic balance (EDB) under varying RH conditions. Their results show that crystalline sucrose barely adsorbs any water before the deliquescence point of 85.6%. They also show that sucrose does not exhibit any efflorescence upon drying, but rather assumes an amorphous, or glassy, state instead. On subsequent humidification cycles the amorphous sucrose particle did not show any significant water uptake before RH of 35-40%. Our present work confirms this observation as the lack of changes in the C 1s and O 1s binding energies and O to C ratio with increasing RH indicates insignificant water uptake by sucrose aerosol particles at low RH below 16%.

### C. Malonic Acid

Figure 7 and figure 8 show the recorded C 1s and O 1s XPS spectra of deposited malonic acid aerosol particles at different relative humidities. The C 1s spectra were fitted with three main peaks corresponding to C-C/C-H originating from the adventitious carbon, COOH from malonic acid and C-C from malonic acid at 285.5 eV, 289.8 eV and 285.8 eV in UHV conditions, respectively. The adventitious carbon C-C/C-H and the malonic acid COOH peaks were not fixed in energy, and the malonic acid C-C peak was fixed at 4.0 eV lower binding energy than the COOH peak. The intensity of the malonic acid C-C peak was fixed to half of that of the COOH peak to reflect the expected stoichiometry of malonic acid. Malonic acid has been shown to be prone to beam damage when exposed to radiation from laboratory x-ray sources. This gives rise to additional peaks in the XPS spectra of malonic acid due to molecules damaged by the x-ray beam, as noted by Ferreira *et al.* [39, 40]. These peaks (denoted DP1 and DP2 following the notation of Ferreira *et al.*) were also included in the fit for 0% RH (UHV), where a good fit could not be produced without. They were fixed to be at 1.5 eV (DP1) and 1.2 eV (DP2) higher binding energies than the C-C and COOH peaks of malonic acid, respectively. In UHV conditions the DP1 and DP2 peaks were observed at 291.3 eV and 287.0 eV. The spectra recorded with water vapor did not show clear indication of the DP2 feature, but an additional peak needs to be fitted close to the DP1 feature in both 0.6% and 3.2% RH spectra. This feature was let to vary freely in energy and intensity, but the shape was fixed to be the same as for the other lines in the spectra. The best fit was acquired with the feature at 286.8 eV and 286.2 eV for 0.6% and 3.2% RH, respectively. This is 1.4 eV higher than the C-C peak of malonic acid in both cases, in good agreement with the position of the DP1 peak of Ferreira *et al.*

The O 1s spectra were fitted with two main peaks for the C=O and C-OH bound oxygen of the two carboxyl groups. The best fit was acquired in UHV for a splitting of approximately 1.0 eV between the C=O and C-OH peaks (532.0 and 533.0 eV, respectively). The splitting is smaller than the previously reported values of 1.1 and 1.3 eV by Ferreira *et al.* For the measurements with water vapor the best fits were obtained with a splitting of 1.2 eV between the C=O and C-OH peaks (531.6 and 532.8 eV at 3.2% RH, respectively), now in good agreement with the work of Ferreira *et al.* The peak at the highest binding energy in the spectra recorded at humid conditions is the O 1s peak from the water vapor. While peaks due to possible beam damage (DP1 and DP2) were observed in the C 1s spectra of malonic acid, fitting corresponding peaks on the O 1s spectrum did not yield in a better representation of the measured

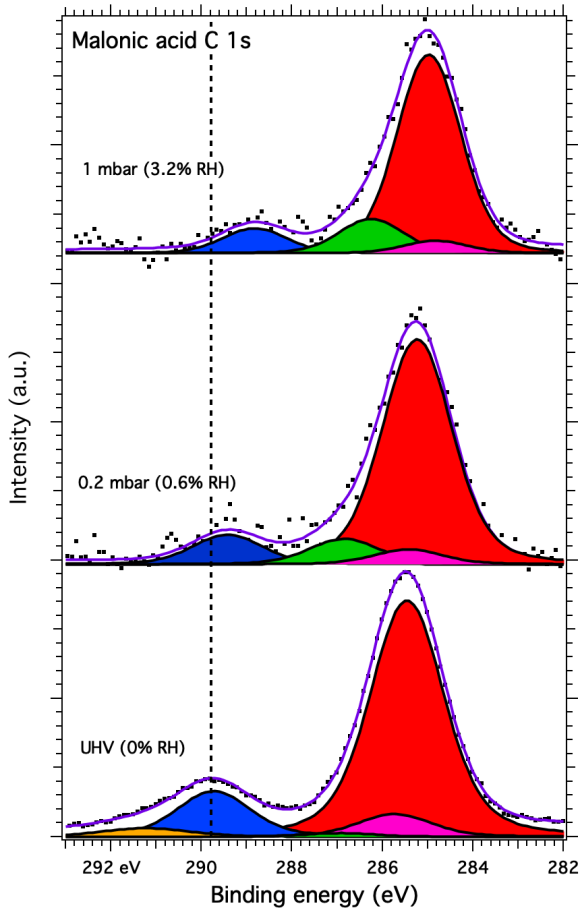


Figure 7. C 1s spectra of malonic acid aerosol particles. The dots show the recorded data, the solid lines the fit envelope curve and the red, blue, green and yellow peaks the C-C/C-H, COOH, DP2 and DP1 components, respectively. The purple peak shows the C-C peak of malonic acid as fixed to the COOH. The dashed vertical line shows the binding energy of the COOH component at 0 mbar pressure (0% relative humidity) in the beginning of the experiments.

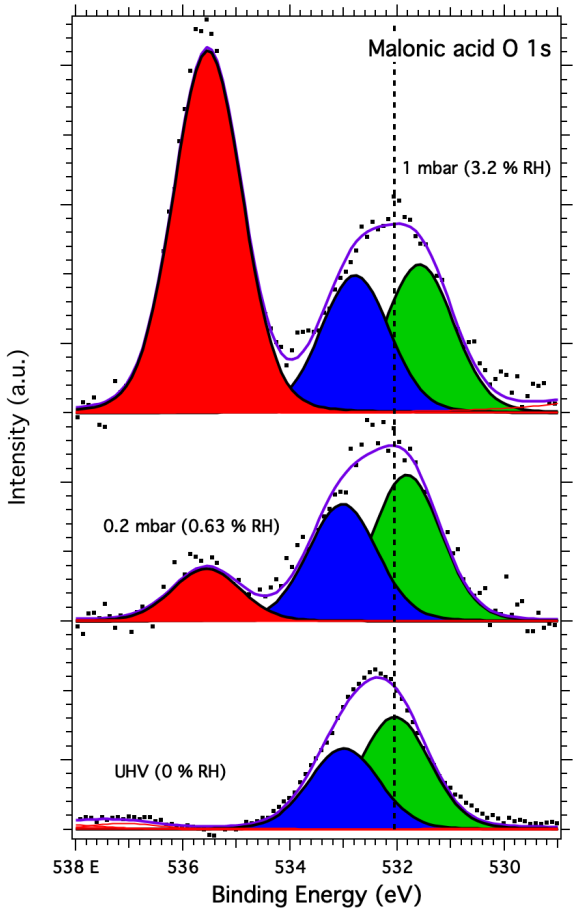


Figure 8. O 1s spectra of malonic acid aerosol particles. The dots show the recorded data, the solid lines the fit envelope curve and the red, blue and green peaks the water vapor, C-OH and C=O components, respectively. The dashed vertical line shows the binding energy of the C=O component at 0 mbar pressure (0% relative humidity) in the beginning of the experiments.

spectra. However, the previous works by Ferreira *et al.* show that the signal due to beam damage is much less pronounced in the O 1s spectra than it is in the C 1s spectra.

When RH is increased, the COOH (and thus also C-C) peak of malonic acid is seen to shift towards lower binding energies with increasing RH. These shifts are presented in Figure 3. While the the shift for O 1s is not as dramatic as for NaCl, the C 1s binding energies shift is even more pronounced than that of Na 1s or Cl 2p of NaCl indicating that water is being adsorbed onto the surface of the aerosol and that the chemical environment of the surface molecules has changed. In addition to the peaks shifts, the C 1s to O 1s signal ratio (O(COOH):C(COOH)) changes within the carboxyl group with increasing RH. The ratio O(COOH):C(COOH) was chosen as the C-C/C-H contribution is under the strong C-C/C-H signal from adventitious carbon and cannot therefore be fitted reliably. The expected stoichiometric ratio of a carboxyl group is 2. Interestingly, already at 0% RH (UHV), the extracted ratio O(COOH):C(COOH)= 1.2 is far from the expected. When introducing water vapor into the system with RH of 0.6% RH, the ratio becomes 2.4, closer to the stoichiometry of a carboxyl group. At 3% RH it becomes even larger with O(COOH):C(COOH)= 3.1. While no clear explanation for this can be offered at the present, it is safe to conclude, based on the observed binding energy shifts and the changes in the O(COOH):C(COOH) ratio, that water is adsorbed on nanoscale malonic acid aerosols particles already at very low RH, and that it has an effect on the chemical composition of the surface of the aerosol.

Looking at the spectra more carefully, it is clear that at 0% RH (UHV) the C 1s spectrum resembles that of a beam damaged sample as described by Ferreira *et al*, but not entirely: the DP2 feature is stronger than reported by Ferreira *et al.* and the DP1 weaker. When increasing the RH, the stronger DP2 peak disappears and only the extra feature attributed to DP1 is seen. The O 1s spectrum does not show any signs of beam damage even at increased RH, but instead the relative intensities between the C=O and C-OH components change more towards the expected (C=O:C-OH) ratio of 1 instead of C=O:C-OH = 1.4 observed at 0% RH (UHV). This indicates an increase in the number of C-OH and decrease in the number of C=O groups with increasing RH. Indeed, the binding energy of the C 1s extra (DP2) feature is close to the typical binding energy (approximately 286.5 eV) of a hydroxyl group, C-OH. If this were purely a result of beam damage, the DP2 feature in the C 1s spectrum should also be visible, not to mention the beam damage component in the O 1s spectra. This could therefore also be a sign of significant chemical changes in the malonic acid aerosols.

Malonic acid is known to exhibit keto-enol tautomerism and it has been theoretically predicted that the transition between the two forms can take place through an intramolecular transition in a system of six water molecules and a malonic acid (see e.g. Ref. [41]). The spectromicroscopic experiments of Ghorai *et al.* [42] combining scanning transmission x-ray microscopy with near-edge x-ray absorption fine structure spectroscopy (STXM/NEXAFS) and Fourier transform infrared spectroscopy (FTIR) on submicron malonic acid aerosol particles with varying RH up to 90% have shown experimentally that while the keto form is dominating in dilute aqueous solutions of malonic acid, the equilibrium shifts toward the enol form in saturated solutions. This observation is also supported by the theoretical calculations of Dick-Perez *et al.* [43] for concentrated malonic acid particles. The results of Ghorai *et al.* show that the amount of enol form increases with increasing relative humidity as water is adsorbed onto malonic acid aerosols. Furthermore they demonstrate water uptake by malonic acid aerosols already at RH as low as 2%, which is in good agreement with the conclusion of the present work. The single particle carbon K-edge NEXAFS spectra of Ghorai *et al.* show a clear increase in C=C and C-OH resonances, while C-COOH and C-CH are decreased with increasing RH. The oxygen K-edge spectra also shows a clear decrease in the -COOH resonance. This is similar to the observations of the present work, where the O 1s C-OH increases with increasing RH. While a similar increase is observed also in the C 1s for the C-OH (DP1) component, one needs to be more cautious in attributing this to the enol form of malonic acid. The C-OH peak at approximately 286.5 eV is a sign of carbon with a single hydroxyl group, while the malonic acid enol form would have a carbon with two hydroxyl groups bound to it, or HO-C-OH (O-C-O), increasing the binding energy from the 286.5 eV to approximately 288 eV. Although no such peak has been fit to the data in the present work, it cannot be ruled out completely. However, if the changes are due to the formation of the enol tautomer, this could have more profound implications in terms of atmospheric chemistry as the keto and enol forms have differing stabilities and reaction pathways in both the gas and aqueous phases [41].

## IV. CONCLUSIONS

Water uptake onto NaCl, sucrose and malonic acid aerosol particles deposited on silicon and gold substrates was studied using the APXPS technique with a laboratory x-ray source (Al K$\alpha$ and Mg K$\alpha$). We exposed the samples to relative humidities between 0% and 16% at room temperature and recorded the XPS spectra of Na 1s, Cl 2p, C 1s and O 1s core levels. The results show that water is adsorbed onto the aerosol particles already at the very low relative humidities and that there are changes in the chemical environment, and possibly even composition, of the particle surfaces with increasing relative humidity. NaCl shows signs of $Cl^-$ dissolving into the thin water layer as well as a memory effect, in binding energies, when drying back to 0% RH, even after heating the aerosols up to 125 °C. The Cl also appears to return to the crystal lattice of the core of the aerosol as the particle is dried although some water seems to remain on the particle. Sucrose aerosols on the other hand show very little changes when exposed to water vapor. Malonic acid shows a dramatic shift in the C 1s binding energies when exposed to tiny amounts of water (0.2–3% RH) as well as a shift in the O 1s binding energies. Furthermore changes are seen in the relative amounts of C=O and C-OH bound oxygen as well as the emergence of a C-OH bound carbon at the cost of COOH. These changes are in line with earlier observations of very early water uptake in malonic acid aerosols [42] and could even indicate a change in the keto-enol equilibrium of malonic acid within the adsorbed water layer.

The present observations suggest that while sucrose aerosol is relatively passive at low RH conditions, the adsorption of very thin layers of water on NaCl and malonic acid aerosols will already have implications in atmospheric chemistry on a molecular level. For example $Cl^-$ ions from sea salt aerosols are a source of chlorine in the troposphere through heterogeneous conversion to chlorines and chlorides (see e.g. Ref. [44] and references therein). With sea salt being one of the most abundant inorganic aerosols in the atmosphere, this implicates possibly significant reactive uptake of

atmospheric trace gases even at low RH. Dicarboxylic acids, like malonic acid, are also ubiquitous in atmospheric aerosols in the troposphere. The fact that they could form concentrated solutions with the enol form present can have implications on the reactivity of these aerosol surfaces.

Our findings demonstrate that APXPS is a valid technique in aerosol research. It can be be utilized, for example, to gain specific, molecular level chemical information about aerosol surfaces, both inorganic and organic, *in situ* at varying relative humidity conditions. We have shown that APXPS can be used on real nanometer-scale aerosols even, when using a conventional laboratory x-ray source. Therefore APXPS using synchrotron radiation shows great promise for studying aerosol surfaces at even higher pressure conditions, more reactive environments as well as with high time resolution.

## CONFLICTS OF INTEREST

There are no conflicts to declare.

## ACKNOWLEDGEMENTS

This project has received funding from the European Research Council (ERC) under the European Union's Horizon 2020 research and innovation programme, Project SURFACE (Grant Agreement No. 717022). The authors also gratefully acknowledge the financial contribution from the Academy of Finland, including Grant Nos. 308238, 314175, 290145, 326291. We thank the staff of MAX IV Laboratory for their assistance during the experiments. We thank Jenny Rissler and Birgitta Svenningsson for assistance with preparation of samples and estimation of surface coverage.

[1] M J Rood, M A Shaw, T V Larson, and D S Covert. Ubiquitous nature of ambient metastable aerosol. *Nature*, 337(6207):537–539, February 1989.

[2] Thien Khoi V Nguyen, Qi Zhang, Jose L Jimenez, Maxwell Pike, and Annmarie G Carlton. Liquid Water: Ubiquitous Contributor to Aerosol Mass. *Environmental Science & Technology Letters*, page acs.estlett.6b00167, June 2016.

[3] S. M. Kreidenweis and A Asa-Awuku. Aerosol Hygroscopicity: Particle Water Content and Its Role in Atmospheric Processes. In Heinrich D Holland and Karl K Turekian, editors, *Treatise on Geochemistry*, pages 331–361. Elsevier, Oxford, 2014.

[4] Mingjin Tang, Chak K Chan, Yong Jie Li, Hang Su, Qingxin Ma, Zhijun Wu, Guohua Zhang, Zhe Wang, Maofa Ge, Min Hu, et al. A review of experimental techniques for aerosol hygroscopicity studies. *Atmospheric Chemistry and Physics*, 19(19):12631–12686, 2019.

[5] Merete Bilde and Birgitta Svenningsson. CCN activation of slightly soluble organics: the importance of small amounts of inorganic salt and particle phase. *Tellus B*, 56(2):128–134, 2004.

[6] Andrew P Ault and Jessica L Axson. Atmospheric aerosol chemistry: Spectroscopic and microscopic advances. *Analytical Chemistry*, 89(1):430–452, 2016.

[7] Miquel Salmeron and Robert Schlögl. Ambient pressure photoelectron spectroscopy: A new tool for surface science and nanotechnology. *Surface Science Reports*, 63(4):169–199, 2008.

[8] D Frank Ogletree, Hendrik Bluhm, Eleonore D Hebenstreit, and Miquel Salmeron. Photoelectron spectroscopy under ambient pressure and temperature conditions. *Nuclear Instruments and Methods in Physics Research Section A: Accelerators, Spectrometers, Detectors and Associated Equipment*, 601(1-2):151–160, 2009.

[9] David E Starr, Hendrik Bluhm, Zhi Liu, Axel Knop-Gericke, and Michael Hävecker. Application of ambient-pressure X-ray photoelectron spectroscopy for the *in-situ* investigation of heterogeneous catalytic reactions. In In-situ *characterization of heterogeneous catalysts*, pages 315–343. Wiley-VCH, 2013.

[10] Lauri Hautala, Kari Jänkälä, Mikko-Heikki Mikkelä, Paavo Turunen, Nønne L Prisle, Minna Patanen, Maxim Tchaplyguine, and Marko Huttula. Probing RbBr solvation in freestanding sub-2 nm water clusters. *Physical Chemistry Chemical Physics*, 19(36):25158–25167, 2017.

[11] N L Prisle, N Ottosson, G Öhrwall, J Söderström, M Dal Maso, and O Björneholm. Surface/bulk partitioning and acid/base speciation of aqueous decanoate: direct observations and atmospheric implications. *Atmospheric Chemistry and Physics*, 12(24):12227–12242, 2012.

[12] M M Walz, C Caleman, J Werner, V Ekholm, D Lundberg, N L Prisle, Gunnar Öhrwall, and Olle Björneholm. Surface behavior of amphiphiles in aqueous solution: a comparison between different pentanol isomers. *Physical Chemistry Chemical Physics*, 17(21):14036–14044, May 2015.

[13] Anthony R Toribio, Nønne L Prisle, and Anthony S Wexler. Statistical Mechanics of Multilayer Sorption: Surface Concentration Modeling and XPS Measurement. *The Journal of Physical Chemistry Letters*, 9(6):1461–1464, February 2018.

[14] Bernd Winter. Liquid microjet for photoelectron spectroscopy. *Nuclear Instruments and Methods in Physics Research Section A: Accelerators, Spectrometers, Detectors and Associated Equipment*, 601(1-2):139–150, March 2009.

[15] Daniel M Murphy, Karl D Froyd, Huisheng Bian, Charles A Brock, Jack E Dibb, Joshua P DiGangi,

Glenn Diskin, Maximillian Dollner, Agnieszka Kupc, Eric M Scheuer, et al. The distribution of sea-salt aerosol in the global troposphere. *Atmospheric Chemistry and Physics*, 19(6):4093–4104, 2019.

[16] M Kanakidou, J H Seinfeld, S N Pandis, I Barnes, F J Dentener, M C Facchini, R Van Dingenen, B Ervens, A Nenes, C J Nielsen, E Swietlicki, J P Putaud, Y Balkanski, S Fuzzi, J Horth, G K Moortgat, R Winterhalter, C E L Myhre, K Tsigaridis, E Vignati, E G Stephanou, and J Wilson. Organic aerosol and global climate modelling: a review. *Atmospheric Chemistry and Physics*, 5(4):1053–1123, 2005.

[17] Joachim Schnadt, Jan Knudsen, Jesper N Andersen, H Siegbahn, A Pietzsch, Franz Hennies, Niclas Johansson, N Mårtensson, G Öhrwall, S Bahr, S Mahl, and O Schaff. The new ambient-pressure X-ray photoelectron spectroscopy instrument at MAX-lab. *J. Synchrotron Rad (2012). 19, 701-704 [doi:10.1107/S0909049512032700]*, 19(5):1–4, August 2012.

[18] Jan Knudsen, Jesper N Andersen, and Joachim Schnadt. A versatile instrument for ambient pressure x-ray photoelectron spectroscopy: The Lund cell approach. *Surface Science*, 646(C):160–169, April 2016.

[19] Samuli Urpelainen, C Såthe, W Grizolli, Marcus Agåker, Ashley R Head, Margit Andersson, Shih-Wen Huang, Brian N Jensen, Erik Wallén, Hamed Tarawneh, Rami Sankari, Ralf Nyholm, Mirjam Lindberg, Peter Sjöblom, Niclas Johansson, Benjamin N Reinecke, M Alif Arman, Lindsay R Merte, Jan Knudsen, Joachim Schnadt, Jesper N Andersen, and Franz Hennies. The SPECIES beamline at the MAX IV Laboratory: a facility for soft X-ray RIXS and APXPS. *Journal of Synchrotron Radiation*, 24(1):344–353, January 2017.

[20] Ignatius N Tang and Harry R Munkelwitz. Composition and temperature dependence of the deliquescence properties of hygroscopic aerosols. *Atmospheric Environment. Part A. General Topics*, 27(4):467–473, March 1993.

[21] Matthew T Parsons, Jackson Mak, Sarah R Lipetz, and Allan K Bertram. Deliquescence of malonic, succinic, glutaric, and adipic acid particles. *Journal of Geophysical Research*, 109(D6):n/a–n/a, March 2004.

[22] Wei Yao, Xin Yu, Joo Won Lee, Xiaoda Yuan, and Shelly J Schmidt. Measuring the deliquescence point of crystalline sucrose as a function of temperature using a new automatic isotherm generator. *International journal of food properties*, 14(4):882–893, 2011.

[23] E. Kukk, G. Snell, J. D. Bozek, W.-T. Cheng, and N. Berrah. Vibrational structure and partial rates of resonant auger decay of the N $1s \rightarrow 2\pi$ core excitations in nitric oxide. *Phys. Rev. A*, 63:062702, May 2001.

[24] E Kukk, K Ueda, U Hergenhahn, X-J Liu, G Prümper, H Yoshida, Y Tamenori, C Makochekanwa, T Tanaka, M Kitajima, et al. Violation of the Franck-Condon principle due to recoil effects in high energy molecular core-level photoionization. *Physical review letters*, 95(13):133001, 2005.

[25] JJ Yeh and I Lindau. Atomic subshell photoionization cross sections and asymmetry parameters: $1 \leqslant z \leqslant 103$. *Atomic Data and Nuclear Data Tables*, 32(1):1–155, 1985.

[26] A Muñoz, JC Oller, F Blanco, JD Gorfinkiel, P Limao-Vieira, and Gustavo García. Electron-scattering cross sections and stopping powers in $h_2o$. *Physical Review A*, 76(5):052707, 2007.

[27] Albert Verdaguer, Juan José Segura, Jordi Fraxedas, Hendrik Bluhm, and Miquel Salmeron. Correlation between charge state of insulating NaCl surfaces and ionic mobility induced by water adsorption: a combined ambient pressure X-ray Photoelectron Spectroscopy and Scanning Force Microscopy study. *The Journal of Physical Chemistry C*, 112(43):16898–16901, 2008.

[28] Q Dai, J Hu, and M Salmeron. Adsorption of water on NaCl (100) surfaces: Role of atomic steps. *The Journal of Physical Chemistry B*, 101(11):1994–1998, 1997.

[29] Steven J Peters and George E Ewing. Thin film water on NaCl(100) under ambient conditions: An infrared study. *Langmuir*, 13(24):6345–6348, 1997.

[30] Michelle C Foster and George E Ewing. Adsorption of water on the NaCl(001) surface. II. An infrared study at ambient temperatures. *The Journal of Chemical Physics*, 112(15):6817–6826, 2000.

[31] Pepa Cabrera-Sanfelix, Daniel Sanchez Portal, Albert Verdaguer, George R Darling, Miquel Salmeron, and Andres Arnau. Spontaneous emergence of $Cl^-$ anions from NaCl(100) at low relative humidity. *The Journal of Physical Chemistry C*, 111(22):8000–8004, 2007.

[32] Albert Verdaguer, GM Sacha, Mónica Luna, D Frank Ogletree, and Miquel Salmeron. Initial stages of water adsorption on NaCl (100) studied by scanning polarization force microscopy. *The Journal of chemical physics*, 123(12):124703, 2005.

[33] D Emfietzoglou and M Moscovitch. Inelastic collision characteristics of electrons in liquid water. *Nuclear Instruments and Methods in Physics Research Section B: Beam Interactions with Materials and Atoms*, 193(1-4):71–78, 2002.

[34] Steven J Peters and George E Ewing. Water on salt: An infrared study of adsorbed $H_2O$ on NaCl(100) under ambient conditions. *The Journal of Physical Chemistry B*, 101(50):10880–10886, 1997.

[35] Sutapa Ghosal and John C Hemminger. Surface adsorbed water on NaCl and its effect on nitric acid reactivity with NaCl powders. *The Journal of Physical Chemistry B*, 108(37):14102–14108, 2004.

[36] Christian George, Markus Ammann, Barbara D'Anna, DJ Donaldson, and Sergey A Nizkorodov. Heterogeneous photochemistry in the atmosphere. *Chemical Reviews*, 115(10):4218–4258, 2015.

[37] Joanna S Stevens and Sven L M Schroeder. Quantitative analysis of saccharides by X-ray photoelectron spectroscopy. *Surface and Interface Analysis*, 41(6):453–462, June 2009.

[38] Bernhard Zobrist, Vacharaporn Soonsin, Bei P Luo, Ulrich K Krieger, Claudia Marcolli, Thomas Peter, and Thomas Koop. Ultra-slow water diffusion in aqueous sucrose glasses. *Physical Chemistry Chemical Physics*, 13(8):3514–3526, 2011.

[39] José M Ferreira Jr, Gustavo F Trindade, Rene Tshulu, John F Watts, and Mark A Baker. Introduction to a series of dicarboxylic acids analyzed by x-ray

photoelectron spectroscopy. *Surface Science Spectra*, 24(1):011001, 2017.

[40] Josè M Ferreira Jr, Gustavo F Trindade, Rene Tshulu, John F Watts, and Mark A Baker. Dicarboxylic acids analysed by x-ray photoelectron spectroscopy, part i-propanedioic acid anhydrous. *Surface Science Spectra*, 24(1):011101, 2017.

[41] Shinichi Yamabe, Noriko Tsuchida, and Kenta Miyajima. Reaction paths of keto–enol tautomerization of $\beta$-diketones. *The Journal of Physical Chemistry A*, 108(14):2750–2757, 2004.

[42] Suman Ghorai, Alexander Laskin, and Alexei V Tivanski. Spectroscopic evidence of keto–enol tautomerism in deliquesced malonic acid particles. *The Journal of Physical Chemistry A*, 115(17):4373–4380, 2011.

[43] Marilú Dick-Pérez and Theresa L Windus. Computational study of the malonic acid tautomerization products in highly concentrated particles. *The Journal of Physical Chemistry A*, 121(11):2259–2264, 2017.

[44] Xuan Wang, Daniel J Jacob, Sebastian D Eastham, Melissa P Sulprizio, Lei Zhu, Qianjie Chen, Becky Alexander, Tomás Sherwen, Mathew J Evans, Ben H Lee, et al. The role of chlorine in global tropospheric chemistry. *Atmospheric Chemistry and Physics*, 19(6):3981–4003, 2019.